

Shape Analysis Using the Fisher-Rao Riemannian Metric: Unifying Shape Representation and Deformation

Adrian Peter¹ and Anand Rangarajan²

¹Dept. of ECE, ²Dept. of CISE, University of Florida, Gainesville, FL

Abstract— We show that the Fisher-Rao Riemannian metric is a natural, intrinsic tool for computing shape geodesics. When a parameterized probability density function is used to represent a landmark-based shape, the modes of deformation are automatically established through the Fisher information of the density. Consequently, given two shapes parameterized by the same density model, the geodesic distance between them under the action of the Fisher-Rao metric is a convenient shape distance measure. It has the advantage of being an intrinsic distance measure and invariant to reparameterization. We first model shape landmarks using a Gaussian mixture model and then compute geodesic distances between two shapes using the Fisher-Rao metric corresponding to the mixture model. We illustrate our approach by computing Fisher geodesics between 2D corpus callosum shapes. Shape representation via the mixture model and shape deformation via the Fisher geodesic are hereby unified in this approach.

I. INTRODUCTION

Deformable models are tremendously important in medical image analysis. For example, shape comparison across subjects and modalities require the computation of similarity measures which in turn rely upon non-rigid deformation parameterizations. Almost all of the previous work in this area uses separate models for shape representation and deformation. The principal goal of this paper is to show that shape representations beget shape deformation parameterizations. This unexpected unification directly leads to a shape comparison measure.

The tremendous body of existing work in shape analysis resists simple taxonomies and summaries. Shape deformation parameterizations range from Procrustean metrics [1] to spline-based models [2], [3], and from PCA-based modes of deformation [4] to landmark diffeomorphisms [5], [6]. Shape representations range from unstructured point-sets [7], [8] to weighted graphs [9] and include curves, surfaces and other geometric models. The one commonality in virtually all of this previous work is that shape representations and deformations do not usually spring from the same model.

In this paper, we use probabilistic models for shape representation. Specifically, Gaussian mixture models (GMM) are used to represent unstructured landmarks for a pair of shapes. Since the two density functions are from the same parameterized family of densities, we use the Fisher-Rao Riemannian metric to construct a geodesic between them. The Fisher-Rao metric is actually the Fisher information matrix of the GMM. To motivate the use of the Fisher-Rao metric, assume for the moment that a deformation applied to a set of landmarks

creates a slightly warped set. The new set of landmarks can also be modeled using another mixture model. In the limit of infinitesimal deformations, the Kullback-Leibler (KL) distance between the two densities is a quadratic form with the Fisher information matrix playing the role of the metric tensor. Using this fact, we can compute a geodesic distance between two mixture models (with the same number of parameters). With mixture models used for shape representation and the Fisher-Rao metric used to compute shape geodesics (deformations), we have a unified shape representation and deformation model. We illustrate our approach by computing Fisher geodesics between 2D corpus callosum shapes.

II. FISHER-RAO RIEMANNIAN METRIC AND INTRINSIC REPRESENTATION

In this section we detail some of the historical context and well-known properties of the Fisher information measure. The Fisher information matrix arises from multi-parameter densities, where the (i, j) entry of the matrix is given by

$$g_{ij}(\theta) = \int p(\mathbf{x}|\theta) \frac{\partial}{\partial \theta^i} \log p(\mathbf{x}|\theta) \frac{\partial}{\partial \theta^j} \log p(\mathbf{x}|\theta) dx. \quad (1)$$

Intuitively one can think of the Fisher information as a *measure of the amount of information present in the data about a parameter θ* .

The Fisher information matrix also satisfies the properties of a metric on a Riemannian manifold. This was first established by Rao [10] and thus leads to our nomenclature of *Fisher-Rao* metric whenever the information matrix is used in this geometric manner. The Fisher-Rao metric is an intrinsic measure, allowing us to analyze a finite, n -dimensional statistical manifold M without considering how M sits in an \mathbb{R}^{n+1} space. In this parametric, statistical manifold, $p \in M$ is a probability density with its local coordinates defined by the model parameters. For example, a bivariate Gaussian density can be represented as a single point on 4-dimensional manifold with coordinates $\theta = (\mu_1, \mu_2, \sigma_1, \sigma_2)^T$, where as usual these represent the mean and standard deviation of the density. The exploitation of the Fisher-Rao metric on statistical manifolds is part of the overarching theory of information geometry [11]. Its utility is largely motivated by Čencov’s theorem [12] which proved that the Fisher-Rao metric is the only metric that is invariant under mappings referred to as congruent embeddings by Markov morphisms. In addition to the invariance property, it can also be shown that many of the other common metrics on

probability densities (e.g. Kullback-Leibler, Jensen-Shannon, etc.) can be written in terms of the Fisher-Rao metric given that the densities are close [11]. For example, the Kullback-Leibler distance between a two parametric densities θ and $\theta + \delta\theta$ is proportional to the Fisher-Rao metric g

$$D(p(x|\theta + \delta\theta)||p(x|\theta)) \approx \frac{1}{2}(\delta\theta)^T g \delta\theta. \quad (2)$$

In other words, the Fisher-Rao metric is equal to, within a constant, a quadratic form with the Fisher information playing the role of the Hessian. Thus, given two parametric densities, we can formulate path length between them as

$$s = \int_0^1 g_{ij} \dot{\theta}^i \dot{\theta}^j dt \quad (3)$$

where the standard Einstein summation convention is assumed and $\dot{\theta}^i = \frac{d\theta^i}{dt}$ is the parameter time derivative. Technically (3) is the square of the geodesic distance, but has the same minimizer as $\int_0^1 \sqrt{g_{ij} \dot{\theta}^i \dot{\theta}^j} dt$ [13]. The functional (3) is minimized using standard calculus of variations techniques leading to the following Euler-Lagrange equations

$$\frac{\delta \mathcal{E}}{\delta \theta^k} = -2g_{ki} \ddot{\theta}^i + \left\{ \frac{\partial g_{ij}}{\partial \theta^k} - \frac{\partial g_{ik}}{\partial \theta^j} - \frac{\partial g_{kj}}{\partial \theta^i} \right\} \dot{\theta}^i \dot{\theta}^j = 0. \quad (4)$$

This can be rewritten in the more standard form

$$g_{ki} \ddot{\theta}^i + \Gamma_{k,ij} \dot{\theta}^i \dot{\theta}^j = 0 \quad (5)$$

where $\Gamma_{k,ij} \stackrel{\text{def}}{=} \frac{1}{2} \left\{ \frac{\partial g_{ik}}{\partial \theta^j} + \frac{\partial g_{kj}}{\partial \theta^i} - \frac{\partial g_{ij}}{\partial \theta^k} \right\}$ is the Christoffel symbol of the first kind. This is a highly non-linear system of PDEs and not analytically solvable. One can use gradient descent to find a local solution to the system with update equations

$$\theta_{\tau+1}^k(t) = \theta_{\tau}^k(t) - \alpha_{\tau} \frac{\delta E}{\delta \theta_{\tau}^k(t)}, \forall t \quad (6)$$

where τ represents the iteration step and α the step size.

These established statistical and geometric properties of the information matrix provide a launch pad for its application to the problem of medical shape analysis. To our knowledge, there have been only two other recent uses of the Fisher-Rao metric for image analysis. The first by Maybank [14], utilizes Fisher information for line detection. The second by Mio *et al.* [15], applies non-parameteric Fisher-Rao metrics for image segmentation. We carefully leverage the discussed results to choose a shape representation that immediately binds the shapes through an intrinsic path. This was alluded to in the above example where we represented the parameters of a Gaussian as a single point on a statistical manifold. We extend this idea by using a mixture-model representation to model our shapes, i.e. a shape with K -points is represented as a K -component GMM where the landmarks are the means of each component. We choose to only place the Gaussian means on the manifold and thus assume an isotropic variance σ^2 for the landmarks and equal weight priors $\pi_a = \frac{1}{K}, \forall a \in \{1, \dots, K\}$. For landmark matching, we assume correspondence between the shapes is known. This parametric, GMM representation for the 2-D shapes is given by [16]

$$p(\mathbf{x}|\theta) = \frac{1}{2\pi\sigma^2 K} \sum_{a=1}^K \exp\left\{-\frac{\|\mathbf{x} - \phi_a\|^2}{2\sigma^2}\right\} \quad (7)$$

where θ is our set of landmarks, $\phi_a = [\theta^{(2a-1)}, \theta^{(2a)}]^T$ and $\mathbf{x} = [x^{(1)}, x^{(2)}]^T \in \mathbb{R}^2$. As previously stated, θ can be interpreted as a point on a Riemannian manifold M with $\dim(M) = 2K$. The Fisher-Rao metric is given by our representation (7) and we can immediately establish the geodesic path between a pair of shapes by minimizing (3) as previously outlined.

The free parameter in our algorithm is σ and in practice this we select it to control the size of the neighborhood of influence for moving the landmarks along the path, with larger values reflecting coverage of more neighbors per landmark. The solution to (3) gives us a completely intrinsic geodesic on the statistical manifold and its path length computed with the Fisher-Rao metric can be used as measure of similarity between the source and target shapes. Our framework couples both the representation of landmarks and intrinsic path traversed. To our knowledge, this is the first time both the representation and deformation have been unified by a common model.

A. Intuition of Intrinsic Geodesics

Even though we cannot visualize our abstract statistical manifold, we have found it helpful to study the resulting geodesics of basic transformations. Figure 1 illustrates two such examples. In Figure 1(a), we take a square shape with four landmarks as the reference shape and match it to the same shape rotated 210° clockwise. Correspondences between landmarks are numerically labeled. The dashed, straight line represents the initialization path and the solid bell-shaped curve shows the final geodesic between shapes. Notice the resulting geodesic is bent indicating the curved nature of the statistical manifold. Figure 1(b) shows a straight-line shape consisting of 21 landmarks that has been slightly collapsed like a hinge. The bendings are symmetric, as expected and illustrate a hyperbolic quality of the manifold. In both cases, we obtained well-behaved geodesics with curved geometry.

III. EXTRINSIC DEFORMATION

The previous section illustrated the derivation of the Fisher-Rao metric which led to a completely intrinsic model for establishing the geodesic between two landmark shapes on a statistical manifold. Once the geodesic has been found, traversing this path yields a new set of θ 's at each discretized location of t which in turn represents an intermediate, intrinsically deformed landmark shape. We would also like to use the results of our intrinsic model to go back and warp the extrinsic space. We now describe how to extend the intrinsic formulation to drive this desired extrinsic space deformation, which is also a necessity for applying this model for applications such as shape registration.

Notice that the intrinsic deformation of the landmarks only required our θ 's to be parametrized by time. Deformation of the ambient space $\mathbf{x} \in \mathbb{R}^2$, i.e. our shape points, can be accomplished via a straightforward incorporation of the time parameter on to our extrinsic space, i.e.

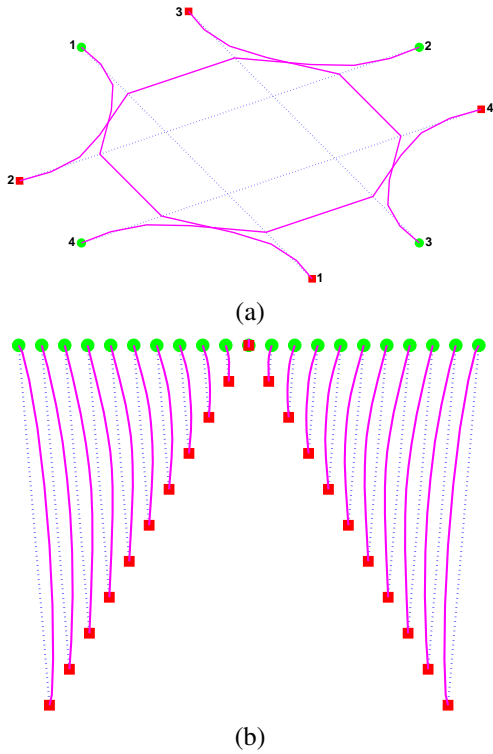


Fig. 1. Basic landmark transformations and their resulting geodesics on statistical manifold. The dashed line is the initialization and the solid line the final geodesic. (a) 4 landmarks, rotation with labeled corresponding landmarks (b) 21 landmarks, straight bending.

$$p(\mathbf{x}(t)|\theta(t)) = \frac{1}{K} \sum_{a=1}^K \frac{1}{2\pi\sigma^2} \exp\left\{-\frac{1}{2\sigma^2} \|\mathbf{x}(t) - \phi_a(t)\|^2\right\}. \quad (8)$$

We want to deform the $\mathbf{x}(t)$'s of extrinsic space through the velocities induced by the intrinsic geodesic and simultaneously preserve the likelihood of all these ambient points relative to our intrinsic θ 's. Instead of enforcing this condition on $L = p(\mathbf{x}(t)|\theta(t))$, we use the negative log-likelihood $-\log L$ of the mixture and set the total derivative with respect to the time parameter to zero:

$$\begin{aligned} \frac{d \log L}{dt} &= (\nabla_{\theta^1} \log L)^T \dot{\theta}^1 + (\nabla_{\theta^2} \log L)^T \dot{\theta}^2 \\ &+ \frac{\partial \log L}{\partial x^1(t)} u - \frac{\partial \log L}{\partial x^2(t)} v = 0 \end{aligned} \quad (9)$$

where $u(t) = \frac{dx^1}{dt}$ and $v(t) = \frac{dx^2}{dt}$ represent the probabilistic flow field induced by our parametric model. Note that this formulation is analogous to the one we find in optical flow problems. Similar to optical flow, we introduce a thin-plate spline regularizer to smooth the flow field

$$\int (\nabla^2 u)^2 + (\nabla^2 v)^2 d\mathbf{x}. \quad (10)$$

We note that it is also possible to use the quadratic variation instead of the Laplacian as the regularizer. On the interior of the grid, both of these satisfy the same biharmonic but the quadratic variation yields smoother flows near the boundaries.

The overall extrinsic space deformation can be modeled using the following energy functional

$$E(u, v) = \int \left(\lambda [(\nabla^2 u)^2 + (\nabla^2 v)^2] + \left[\frac{d \log L}{dt} \right]^2 \right) d\mathbf{x} \quad (11)$$

where λ is a regularization parameter that weighs the error in the extrinsic motion equation relative to the departure from smoothness. The minimal flow fields are obtained via the Euler-Lagrange equation of (11). As formulated the mapping found through the thin-plate regularizer is not guaranteed to be diffeomorphic. This can be enforced if necessary and will be detailed in subsequent work. In this section, we have shown that selecting the representation model (8) immediately gave the likelihood preserving data term used to drive the warping of extrinsic shape points thus continuing our theme of unified shape representation and deformation.

IV. EXPERIMENTAL RESULTS

The shape matching framework detailed in Sections II and III was validated to illustrate two fundamental parts of our algorithm: (1) discovering intrinsic geodesics between landmark representation of shapes and (2) using the geodesic to drive extrinsic deformation. All analysis was conducted on nine corpus callosum shapes consisting of 63 points each, see Figure 3. Shape 1 was used as the reference for all experiments and compared against the remaining eight shapes. Figure 2(a) illustrates an overlay of two candidate shapes with isotropic variances assigned to each shape's landmarks. We use the gradient descent algorithm to find the intrinsic geodesic between corpus callosum pairs. We then compute a shape distance (i.e. similarity metric) between the pairs by integrating along the geodesic using the Fisher-Rao metric. It is worth noting that even though the corpora callosa are simple closed contours, our analysis works on an arbitrary set of landmarks that can include interior curves. Also using the geodesic, we can transport the reference shape to the target shape, validating our unified representation and deformation model. Table I lists a comparative analysis of our shape distance with the thin-plate spline (TPS) bending energy between the shapes. Though some of the distances are close together, we visually verified that larger distances correlated with dissimilar shapes. In these and other experiments, we have noticed a global agreement trend with local variation between the Fisher-Rao and TPS metrics. For example, shapes 4, 7, and 9 differ the most from our reference shape while shapes 2, 3, 5, 6, and 8 resemble it. However, the table shows the Fisher-Rao and TPS differ in their ordering of the degrees of similarity within these groups. This indicates differing sensitivities to the same local deformations which may be very valuable medical analysis.

Following the intrinsic analysis, we next use the geodesic to move the extrinsic space surrounding the landmarks. Figure 2(b) illustrates the resulting warp for matching shape 1 onto shape 2. The ability to warp the extrinsic space will facilitate further medical image analysis including image registration and atlas generation.

Pairs	Fisher-Rao	TPS
1 vs. 2	0.36171	0.07719
1 vs. 3	0.18461	0.01466
1 vs. 4	1.1173	0.10595
1 vs. 5	0.34005	0.08275
1 vs. 6	0.12971	0.04767
1 vs. 7	0.66445	0.13277
1 vs. 8	0.04259	0.03047
1 vs. 9	0.42015	0.12917

TABLE I

PAIRWISE SHAPE DISTANCES. COLUMN 2 IS OBTAINED BY INTEGRATING THE INTRINSIC GEODESIC USING THE FISHER-RAO METRIC. COLUMN 3 IS THE BENDING ENERGY OF THE TPS WARP.

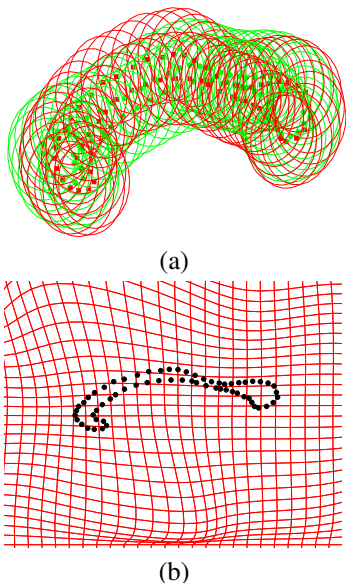


Fig. 2. (a) Isotropic variances assigned to each landmark. (b) Extrinsic space mapping taking shape 1 onto shape 2.

V. DISCUSSION AND FUTURE WORK

We have presented a unified framework for shape representation and deformation. Previous approaches treat representation and deformation as two distinct problems. Our representation of landmark shapes using mixture models enables immediate application of the Fisher information matrix as a Riemannian metric to establish an intrinsic geodesic between shape pairs. Armed with the Fisher-Rao metric, we are able to establish a notion of distance between the shapes on a statistical manifold. We also illustrated how to leverage this path to deform the extrinsic space. Our technique was applied to matching corpus callosum landmarks, illustrating the usefulness of this method for shape discrimination and deformation analysis. The immediate next step is to move beyond landmarks and model shape point-sets using Gaussian mixture models thereby fixing free parameters such as the variance parameter σ^2 . Our future work will focus on extending this framework to incorporate diffeomorphic warping of the extrinsic space and intrinsically solving for correspondences between the shape landmarks.

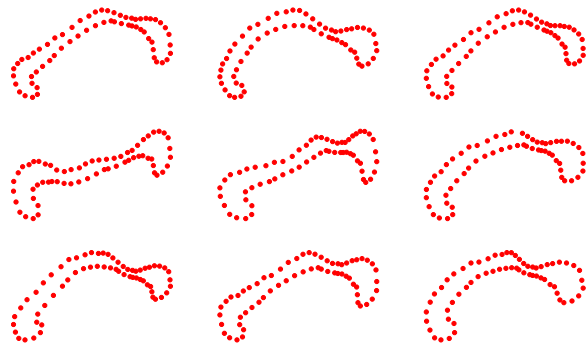


Fig. 3. Nine corpus callosum shapes used for pairwise matching, 63 landmarks per shape. Shape number increases left to right per row.

ACKNOWLEDGEMENTS

This work is partially supported by NSF IIS-0307712. We acknowledge helpful conversations with Hongyu Guo, Eric Spellman and Gnana Bhaskar Tenali. We also thank Harris Corporation for the first author's educational sponsorship.

REFERENCES

- [1] C. Small, *The statistical theory of shape*, Springer, New York, NY, 1996.
- [2] F. L. Bookstein, "Principal warps: Thin-plate splines and the decomposition of deformations," *IEEE Trans. Patt. Anal. Mach. Intell.*, vol. 11, no. 6, pp. 567–585, June 1989.
- [3] R. Sprengel T.M. Buzug J. Weese K. Rohr, H.S. Stiehl and M.H. Kuhn, "Landmark-based elastic registration using approximating thin-plate splines," *IEEE Trans. on Medical Imaging*, vol. 20, no. 6, pp. 526–534, June 2001.
- [4] R.H. Davies, C. Twining, T.F. Cootes, and C.J. Taylor, "An information theoretic approach to statistical shape modelling," in *European Conference on Computer Vision (ECCV)*, 2002, Lecture Notes in Computer Science, LNCS 2351, pp. III: 3–20, Springer.
- [5] V. Camion and L. Younes, "Geodesic interpolating splines," in *Energy Minimization Methods in Computer Vision and Pattern Recognition (EMMCVPR)*, Lecture Notes in Computer Science, LNCS 2134, pp. 513–527. Springer, New York, 2001.
- [6] S. Joshi and M. Miller, "Landmark matching via large deformation diffeomorphisms," *IEEE Trans. Image Processing*, vol. 9, pp. 1357–1370, 2000.
- [7] H. Chui and A. Rangarajan, "A new point matching algorithm for non-rigid registration," *Computer Vision and Image Understanding*, vol. 89, pp. 114–141, 2003.
- [8] H. Guo, A. Rangarajan, S. Joshi, and L. Younes, "Non-rigid registration of shapes via diffeomorphic point matching," in *International Symposium on Biomedical Imaging (ISBI)*, 2004, pp. 924–927, IEEE.
- [9] S. J. Dickinson K. Siddiqi, A. Shokoufandeh and S. W. Zucker, "Shock graphs and shape matching," in *ICCV*, 1998, pp. 222–229.
- [10] C.R. Rao, "Information and accuracy attainable in estimation of statistical parameters," *Bulletin of the Calcutta Mathematical Society*, vol. 37, pp. 81–91, 1945.
- [11] S-I. Amari and H. Nagaoka, *Methods of Information Geometry*, American Mathematical Society, 2001.
- [12] N.N. Cencov, "Statistical decision rules and optimal inference," 1982, American Mathematical Society.
- [13] R. Courant and D. Hilbert, *Methods of Mathematical Physics*, Wiley-Interscience, 1989 (new ed.).
- [14] S.J. Maybank, "The Fisher-Rao metric for projective transformations of the line," *International Journal of Computer Vision*, vol. 63, no. 3, pp. 191–206, 2005.
- [15] W. Mio, D. Badlyans, and X. Liu, "A computational approach to Fisher information geometry with applications to image analysis," in *Energy Minimization Methods in Computer Vision and Pattern Recognition (EMMCVPR)*, Lecture Notes in Computer Science, LNCS 3757, pp. 18–33. Springer, 2005.
- [16] G. J. McLachlan and K. E. Basford, *Mixture models: inference and applications to clustering*, Marcel Dekker, New York, 1988.